OBSERVATIONS AND ANALYSIS OF IONOSPHERIC ELECTRODYNAMICS DURING A SUBSTORM RECOVERY PHASE USING THE MIRACLE NETWORK

O. Amm[1], A. Aksnes[2], J. Stadsnes[2], N. Østgaard[3], R.R. Vondrak[4], G.A. Germany[5], and I. Sillanpää[1]

[1]*Finnish Meteorological Institute, Space Physics Program, P.O. Box 503, FIN-00101 Helsinki, Finland*
tel: +358 9 1929-4689/ fax: +358 9 1929-4603
e-mail: Olaf.Amm@fmi.fi/ Ilkka.Sillanpaa@fmi.fi
[2]*Department of Physics and Technology, University of Bergen, Bergen, Norway*
[3]*University of California, Berkeley, CA 94720-7450, USA*
[4]*NASA/Goddard Space Flight Center, Code 690, Greenbelt, MD 20771, USA*
[5]*University of Alabama, Center for Space Plasma and Aeronomy Research, Huntsville, AL 35899, USA*

ABSTRACT

We present ground-based electromagnetic data from the MIRACLE and BEAR networks and satellite optical observations from the UVI and PIXIE instruments on the Polar satellite of an omega band event over Northern Scandinavia on June 26, 1998, which occurs close to the morning side edge of a substorm auroral bulge. Our analysis of the data concentrates on one omega band period from 0318-0327 UT, for which we use the method of characteristics combined with an analysis of the UVI and PIXIE data to derive a time series of instantaneous, solely data-based distributions of the mesoscale ionospheric electrodynamic parameters with a 1-min time resolution. Our results show that zonally alternating regions of enhanced ionospheric conductances ("tongues") up to ~ 60 S and low conductance regions are associated with the omega bands. The tongues have a poleward extension of ~ 400 km from their base and a zonal extension of ~ 380 km. While they are moving coherently eastward with a velocity of ~ 770 ms^{-1}, the structures are not strictly stationary. The current system of the omega band can be described as a superposition of two parts: One consists of anticlockwise rotating Hall currents around the tongues, and Pedersen currents with a negative divergence in their centers. The sign of this system is reversing in the low conductance areas. It causes the characteristic ground magnetic signature. The second part consists of zonally aligned current wedges of westward flowing Hall currents and is mostly magnetically invisible below the ionosphere. This system dominates the field-aligned current (FAC) pattern and causes alternating upward and downward FAC at the flanks of the tongues with maximum upward FAC of ~ 25 $\mu A\ m^{-2}$. The total FAC of ~ 2 MA are comparable to the ones diverted inside a westward traveling surge (WTS). Throughout the event, the overwhelming part of the FAC are associated with gradients of the ionospheric conductances, and 66-84% of the FAC are connected with ionospheric Hall currents.

INTRODUCTION

Auroral omega bands are periodic, wave-like undulations of the poleward boundary of the morning side diffuse aurora occurring in the recovery phase of substorms. The name omega bands was originally chosen by Akasofu and Kimball (1964) with respect to the dark areas between the poleward extending auroral waves or tongues, which resemble the form of the inverted capital greek letter Ω. The luminous tongues tend to be narrower and having larger latitudinal extent for more intense substorms, and may occasionally develop into auroral torches which are narrow, finger-like auroral forms that extend several degrees of latitude poleward from the auroral oval. Inside the tongues which are primarily deformations of the diffuse auroral boundary, also discrete aurora can be found, especially at the tongues' poleward boundary. Pulsating aurora has been observed inside torches. The typical longitudinal as well as latitudinal extent of the tongues amounts to about 400-500 km. Omega bands have been found to grow simultaneously over a longitudinal range of several magnetic local time (MLT) hours, and have also been observed simultaneously in both hemispheres (Mravlag *et al.*, 1991).

The auroral forms are drifting eastward with velocities ranging between 400 and 2000 ms^{-1}, with a tendency of increasing drift speed with time. These velocities have been found to agree closely with the local $\vec{E}\times\vec{B}$ drift velocity. During their eastward drift, the shape of the auroral forms is essentially preserved, thus indicating a mostly stationary structure in the frame of reference comoving with the forms. A ground magnetometer positioned below the periodic, stationary and moving auroral omega bands measures Ps6 pulsations, i.e., magnetic disturbances with periods of 5-40 min, and amplitudes that may vary from 10 to over 1000 nT. The causal relation between the auroral and the magnetic phenomena was first pointed out by Saito (1978). The ground magnetic pulsations are most prominent in the magnetic Y (eastward) component, in which the maxima are more pronounced than the minima. The maxima in Y occur between respective minima and maxima in the Z (vertical downward) component related to the same omega band, where the Z minima are leading the Y maxima by a phase shift of approximately 90 degrees. In the X (northward) component, the pulsations are also often visible, but they are typically quite disturbed due to the temporal variation of the substorm electrojet intensity during the recovery phase. For more details, see the recent review in Paschmann *et al.* (2003).

INSTRUMENTATION AND OBSERVATIONS

The MIRACLE network of ground-based instruments (Syrjäsuo et al., 1998) consists of the IMAGE magnetometer network (see dots with stars in Figure 1), the renewed STARE coherent scatter radar which measures the ionospheric electric field in the area of the black frame indicated in the Figure, and several all-sky

cameras which are not used in this study due to the northern summer light conditions. For our event on June 26, 1998, in addition to IMAGE, data of the temporary, but very extended BEAR magnetometer network (Korja *et al.*, 2002) are available (see dots in Figure 1). These two networks together provide the densest coverage of magnetometers that has existed in Northern Scandinavia as yet.

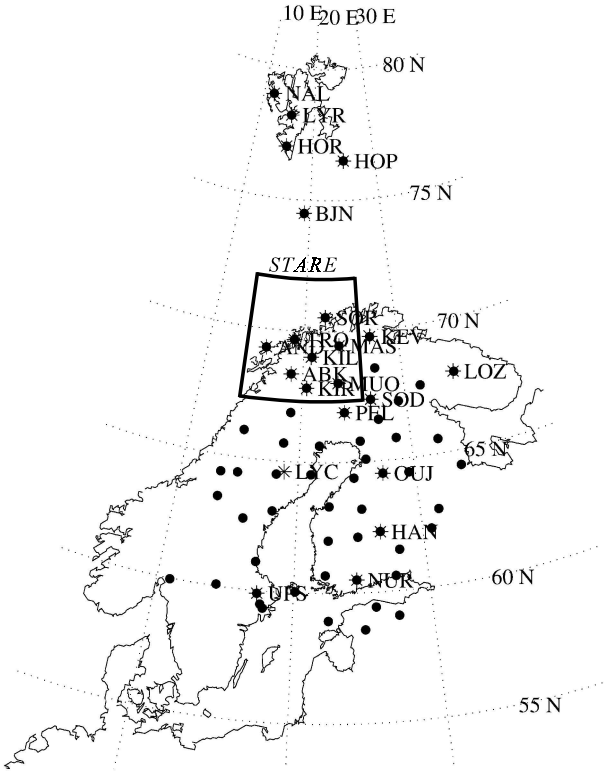


Figure 1. Location of the IMAGE (dots with stars) and BEAR (dots) magnetometer stations in Northern Scandinavia, and the field of view of the STARE radar (black frame).

From remote sensing of the UV- and X-ray aurora, the Ultraviolet Imager (UVI) and the Polar Ionospheric X-ray Imaging Experiment (PIXIE) onboard the Polar satellite can provide instantaneous global maps of the precipitating electrons.

The UVI instrument measures UV-emissions within the Lyman-Birge-Hopfield (LBH) band (140-180 nm), caused mainly by the precipitating electrons impact on N_2. When produced at altitudes below about 150 km, some of the LBH emissions will be absorbed by O_2. The amount of absorption is determined by the O_2 Schumann-Runge absorption continuum, which peaks at the shorter wavelengths and decreases with longer wavelengths. The LBH emissions are thus divided into two bands: A shorter wavelength region of 140-160 nm denoted LBHS, with significant loss due to O_2 absorption, and another region between 160 and 180 nm, LBHL, with less loss. By taking the ratio between the intensities of the two LBH-bands, we can estimate the average precipitating electron energy. As the longest wavelengths are hardly affected by O_2 absorption, the LBHL emissions are further directly proportional to the incident auroral electron energy flux. Using UVI measurements, we are thus able to perform a remote diagnostic of the precipitating electrons in the energy range between approximately 0.1 and 20 keV. The spatial resolution of the UVI camera is nominally ~ 40 km (Torr *et al.*, 1995), but wobbling of the despun platform on the Polar satellite means the spatial resolution is degraded in one direction to ~ 360 km. For more details, see Germany *et al.* (1997; 1998a,b).

The PIXIE camera measures bremsstrahlung in the energy range between approximately 2 and 22 keV (Imhof *et al*., 1995), produced by the interaction between precipitating electrons and the nuclei of atmospheric particles. There exist a well-established relationship between precipitating electrons and the production of X-rays (Evans, 1955). From the derived PIXIE X-ray spectra, a four-parameter representation of the precipitating electron energy spectra can be estimated, having an electron energy range of 5-100 keV and a spatial resolution of 600-900 km (depending on Polar altitude). A detailed description of the procedure is given by Østgaard *et al*. (2000, 2001).

In Figure 2, the spatio-temporal variation of the magnetic field during our analysis interval has been represented by the equivalent current vectors just below the ionospheric plane $\vec{J}_{eq,ion}$ (e.g., Untiedt and Baumjohann, 1993). These vectors have been derived from the ground magnetic disturbance field using the Spherical Elementary Current System (SECS) method (Amm and Viljanen, 1999). During this procedure, $\vec{J}_{eq,ion}$ is partly also derived on areas which are not in an immediate vicinity of the ground magnetometers. The reliability of this approach has been confirmed by Pulkkinen *et al.* (2003). In addition, the colour panels in Figure 2 show the UVI measurements in the area of Northern Scandinavia. As the UVI camera operates alternately with the LBHL and LBHS filters for this event, both image types are alternating in the time series. For the full minutes around which no UVI data are available, only $\vec{J}_{eq,ion}$ is shown. These data are arranged in three different rows such that time proceeds from left to right. When looking at a series of LBHL and LBHS images it is important to keep in mind that the same ionospheric feature may appear somewhat different in them due to their different energy and absorption characteristics as explained above. While the ground-based instruments have a time resolution of 20 s, the UVI integration time is 37 s for our event. In order to make the presentation of $\vec{J}_{eq,ion}$ and the UVI images most consistent, we have averaged $\vec{J}_{eq,ion}$ over the UVI integration time periods in Figure 2.

Also $\vec{J}_{eq,ion}$ shows the typical signature expected for omega bands: The substorm westward (equivalent) electrojet with maximum current amplitudes of ~ 2 Am^{-1} shows a meandering behaviour such that around 0323 UT when a Z component minimum at the IMAGE magnetometer station KIL (data not shown) indicates that the central "tongue" of the omega band is above the station, $\vec{J}_{eq,ion}$ exhibits an anticlockwise vorticity and vectors with larger amplitudes (up to ~ 1.3 Am^{-1}) shift polewards to ~ 71° latitude. Oppositely, around 0326 UT when a Z component maximum indicates that the KIL magnetometer is located in the regions between the tongues, a clockwise vorticity is observed and the largest $\vec{J}_{eq,ion}$ vectors are concentrated at the equatorward border of the area shown in Figure 2. As can most easily be seen from the $\vec{J}_{eq,ion}$ signature of the tongues, the equivalent current

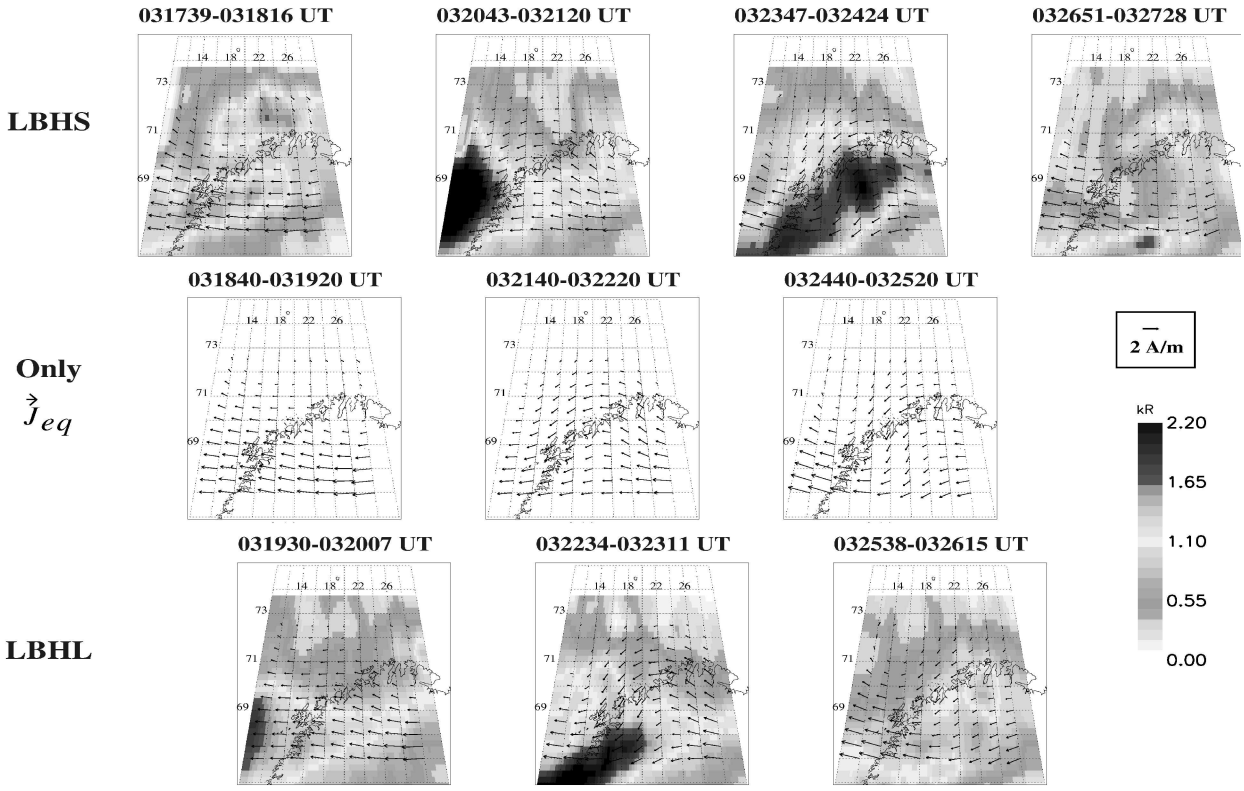


Figure 2. Ionospheric equivalent currents (vectors) and UVI emissions (greyscale plots) for our detailed analysis interval. Plots around full minutes are organised from left to right with proceeding time, and according to the available UVI image: LBHS filter: upper row; LBHL filter: lower row; no UVI images: central row. The equivalent currents are averaged with respect to the UVI integration periods noted above each plot.

structure is moving eastward over the MIRACLE area. From this signature, the velocity can be estimated to ~ 770 m s^{-1}, well in the typical range of omega bands.

The UVI camera on Polar observes an eastward moving form with enhanced intensities reaching about 2.5 kR at most. This form intrudes to the southwestern edge of the displayed area at 0320 UT, and covers the equatorial part of that area up to ~ 71° latitude as a southwest-northeast aligned strip at 0324 UT. This feature is well aligned with the westward flank of the tongue of the omega band as determined from $\vec{J}_{eq,ion}$, and in the LBHS image of 0324 UT it also covers its central part. Outside this intensification the UVI intensities are considerably smaller, particularly at the poleward side of our area. As is to be expected (e.g., Frey *et al.*, 1999), the observed UVI signature is not exactly identical with the Ω type appearance typically seen in visual band optical data. Still, the eastward movement of a tongue-like feature and the darker areas around it are clearly discernable. As the global UVI images indicate (data now shown), the omega bands shown are located at the morning side edge of the substorm auroral bulge.

The STARE radar measures a mainly southward directed electric field $\vec{E}$ (data not shown), with magnitudes varying from ~ 30 - 75 mV m^{-1} where the largest electric field magnitudes are observed at the poleward edge of the omega structures. A negative divergence of $\vec{E}$ is observed during the period when the tongue of the omega band moves through the radar's field of view.

ANALYSIS TECHNIQUES

Two techniques to derive ionospheric conductances are used for our analysis: The two-dimensional (2D) method of characteristics and a technique to derive the conductances from the UVI and PIXIE data. The method of characteristics (Inhester *et al.*, 1992; Amm, 1995, 1998) combines spatial data of $\vec{J}_{eq,ion}$ with data of $\vec{E}$ to solve a differential equation for the Hall conductance Σ_H. For this, an estimate of the Hall to Pedersen conductance ratio α is needed. With the resulting Σ_H and the input data, the true horizontal currents $\vec{J}$ and the field-aligned currents $j_{\parallel}$ can then be calculated. This paper focuses on the discussion of the results of the two-dimensional method of characteristics for the period presented in the previous section. The derivation of the ionospheric Hall and Pedersen conductances from UVI and PIXIE data is here only used for the estimation of α which is assumed uniform in space for a given timestep. This task is perfomed using a computer code developed by the University of Maryland. The code is based on the TANGLE code (Vondrak and Baron, 1976; Vondrak and Robinson, 1985), and it models ionospheric conductances by taking precipitating electron energy spectra as input. A detailed description of the code is provided by Aksnes *et al.* (2002, 2004).

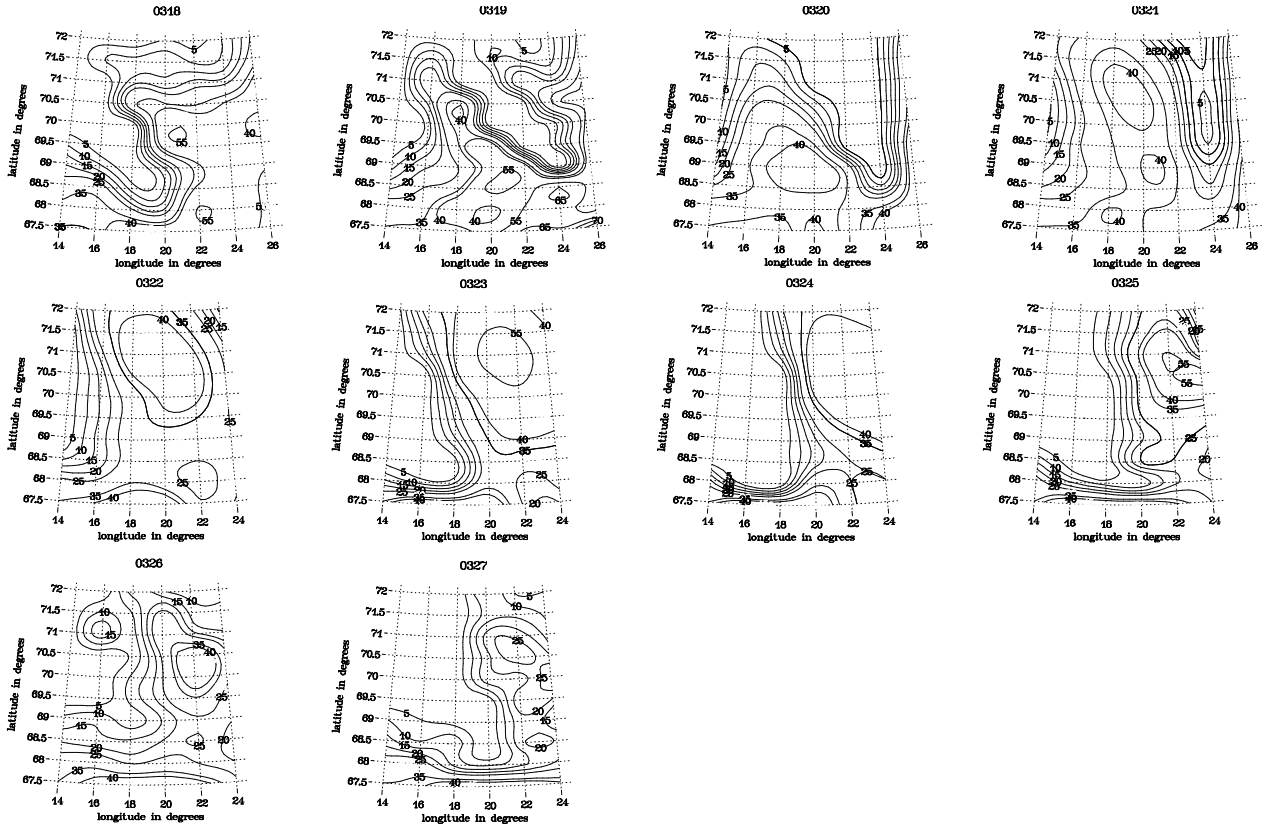


Figure 3a. Analysis results of the method of characteristics: Hall conductance Σ_H.

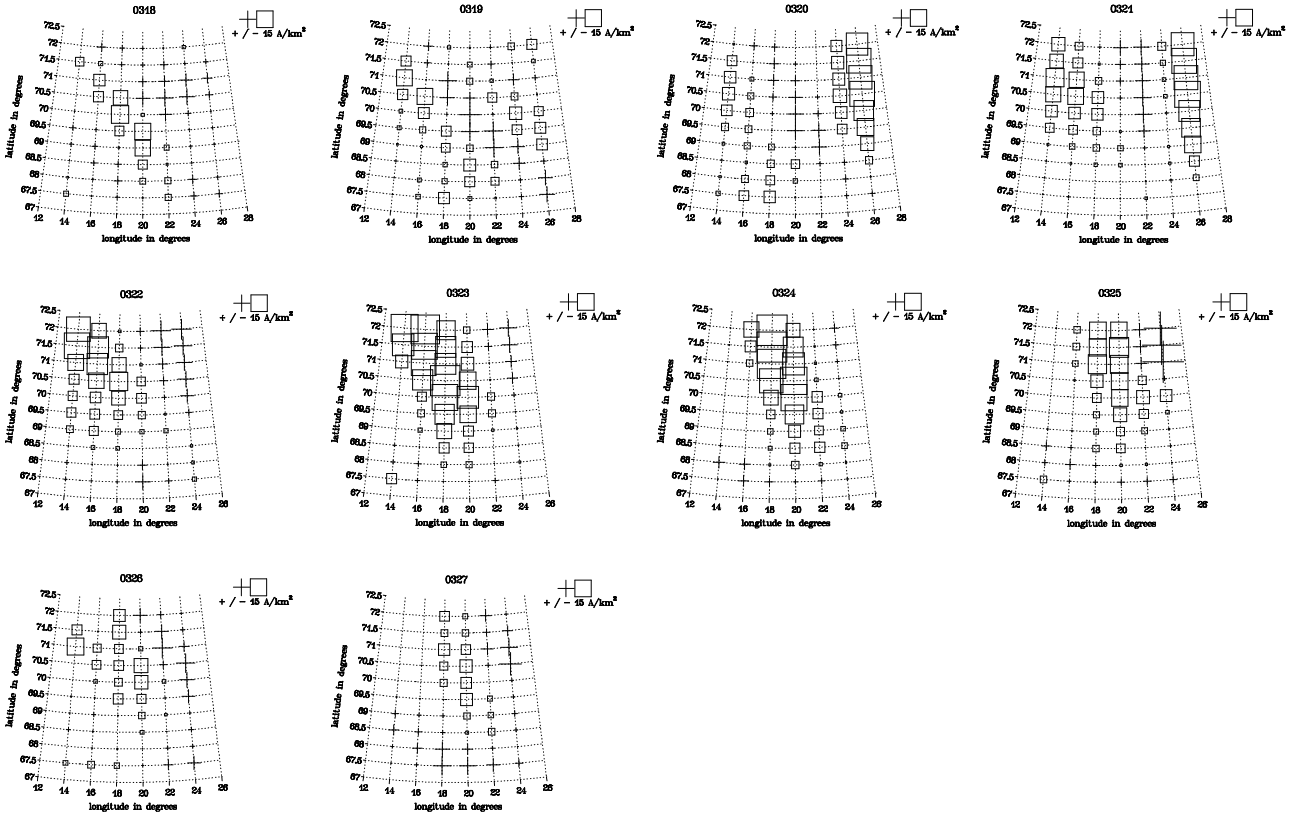


Figure 3b. Analysis results of the method of characteristics: Field-aligned currents (crosses: downward currents; squares: upward currents).

ANALYSIS RESULTS AND DISCUSSION

The results of the analysis with the 2D method of characteristics are displayed as time series in Figure 3. The values of α that resulted from the UVI and PIXIE analysis and which are used for the calculation are 2.75 for 0318-0319 UT, 2.4 for 0320-0325 UT, and 2.3 for 0326-0327 UT. Figure 3a shows the resulting Σ_H distributions, the primary output of the method of characteristics, as isocontour plots. A poleward extending tongue-like region of enhanced Σ_H values, slightly tilted in northwest-southeastern direction, is seen to move eastward over the analysis region from 0319 UT to 0325 UT. The maximum conductances inside the tongue are varying from ~ 40 to 60 S and are located most poleward between 0321 and 0323 UT. Starting from 0326 UT, the maximum Hall conductances in the poleward part of the analysis area decrease, and the appearance of the conductance structure becomes more diffuse. At the flanks on the moving tongue, regions with low Σ_H values below 5 S are visible. Steep conductance gradients, particularly in longitudinal direction, are present between the tongues and the adjacent regions. The second area where enhanced conductances are observed with magnitudes comparable to the maximum ones in the tongues is the equatorward border of our analysis area, the "base" of the omega bands. The conductance structure in this region does not follow the movement of the tongues.

The resulting true ionospheric currents $\vec{J}$ (not shown) are generally pointing southwestward, as a consequence of the mostly southward electric field that generates southward Pedersen and westward Hall currents. The maximum current density reaches to over 4000 mAm^{-1} in the area of the tongues of conductance enhancements around 0323 UT. In response to the steep conductance gradients, similar steep gradients in zonal direction are also seen in $\vec{J}$, except for in the area of the base of the omega bands. The most obvious difference between the equivalent (Figure 2) and the true currents is that the later do not show a meandering signature like the former do, but are essentially disrupted when they encounter a low conductance area, and reappear in the subsequent high conductance area again.

Consequently, this change in $\vec{J}$ needs to be moderated by upward (downward) field-aligned currents $j_\parallel$ (FAC) at the westward (eastward) flank of the high conductance regions (Figure 3b; crosses denote downward, squares upward FAC). Alternating, meridionally aligned (with a slight tilt in northwest-southeast direction) sheets of FAC are visible which are comoving with the conductance tongue structures. The upward FAC vary in magnitude between ~ 15 - 25 μA m^{-2}, while the downward FAC are on average smaller and mostly do not exceed 10 μA m^{-2} (for a more detailed discussion on the FAC balance and current closure see below). These alternating FAC sheets together with the horizontal currents cause the characteristic meandering signature observed in $\vec{J}_{eq,ion}$.

A decomposition of the true ionospheric currents $\vec{J}$ into their curl-free, divergence-free and Laplace (i.e, curls and/or divergences solely outside of the analysis region) parts (cf., Amm, 1996), separately performed for the Hall and Pedersen currents (plots not shown), results into the following subdivision of the omega band current system into two parts on top of the background westward electrojet: One part consists of anticlockwise rotating Hall currents around the tongues, and Pedersen currents with a negative divergence in their centers. The sign of this system is reversing in the low conductance areas. It causes the characteristic ground magnetic signature. The second part consists of zonally aligned current wedges of westward flowing Hall currents and is mostly magnetically invisible below the ionosphere. This system dominates the FAC pattern and causes alternating upward and downward FAC at the flanks of the tongues with maximum upward FAC of ~ 25 μA m^{-2}.

In the following, we analyse some aspects of the FAC system and the current balance in more detail: In Figure 4 we analyse the FAC distribution at 0323 UT by decomposing the total FAC (compare Figure 3b) into

$$j_\parallel = \Sigma_P \, \nabla_h \cdot \vec{E} + \nabla_h \Sigma_P \cdot \vec{E} + \nabla_h \Sigma_H \cdot \left(\hat{z} \times \vec{E}\right)$$

where the subscript 'h' denotes the horizontal part of the nabla operator, and $\hat{z}$ is the unit vector in downward direction. The three terms of the right-hand side of this equation are called "term 1" to "term 3" here. While term 1 is related to the divergence of $\vec{E}$, terms 2 and 3 are proportional to the gradients of the Pedersen and Hall conductance, respectively. Term 1 contributes to upward FAC in the area of the enhanced conductance tongue of up to ~ 4 μA m^{-2} magnitude. Both terms related to the conductance gradients exhibit upward FAC at the western flank of the tongue, and some downward FAC are present at the northeastern edge of the analysis area. However, term 3 related to the gradients of the Hall currents is with upward FAC amplitudes up to ~ 20 μA m^{-2} by far dominating both other terms. This result underlines the importance of the conductance gradients for the resulting current system (as for uniform conductances only term 1 would be non-zero), and the dominating role of the westward directed Hall current wedge for the FAC related to our event. Note that in some studies (e.g., Sofko *et al.*, 1995), term 1 has been called "magnetospheric FAC" while terms 2 and 3 have been named "ionospheric FAC", although it appears difficult to justify such a separation in terminology in a coupled system. While in those studies term 2 and 3 are usually neglected, they contribute more than 85% of the total FAC in our case at 0323 UT.

The above result is further specified for the whole time series of our analysis in Figure 5. The dots show the part of the total FAC that connect to Hall currents ($|\nabla_h \cdot \vec{J}_H|$) in percent (scale on the right side of the graph), integrated over the analysis area. The remainder connects to ionospheric Pedersen currents. Throughout the whole event, the FAC part connecting to Hall currents dominates with ~ 66 - 84%. The crosses denote the absolute FAC ($|j_{\parallel,up}| + |j_{\parallel,down}|$) integrated over the analysis area for each timestep (scale on the left side of the graph). These total absolute FAC are varying from ~ 1.5 MA in the beginning and end of the analysed period to the maximum value of ~ 2.3 MA at 0323 UT. We note that these values are of a similar order of magnitude as the total upward FAC diverted in a westward traveling surge (WTS), the westward end of the substorm electrojet, as estimated to ~ 1 MA by Opgenoorth *et al.* (1983b) and ~ 2.5 MA by Gjerloev and Hoffman (2002). This indicates that a significant part of the substorm electrojet in the morning sector is intermediately disrupted due to the zonally alternating high and low conductance structures related to the omega bands in the morning sector of the substorm auroral bulge. Generally, our results are in good

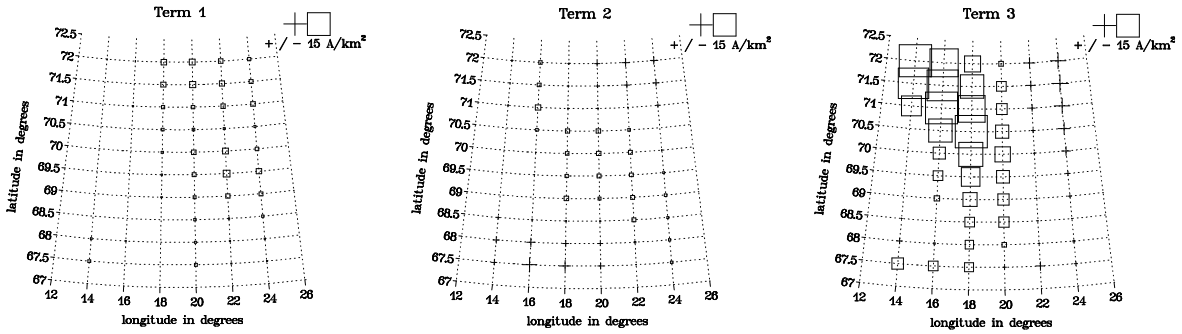


Figure 4. Decomposition of the total FAC density $j_{\parallel}$ at 0323 UT into a term related to the divergences of the electric field (left panel), a term related to the gradients of the Pedersen conductance (middle panel), and a term related to the gradients of the Hall conductance (right panel); crosses denote downward, squares upward currents; for more details see text.

agreement with the finding of Lu (2000) that the FAC connected to the Hall currents amount to ~ 30-50% of the total FAC, seen over the whole substorm bulge.

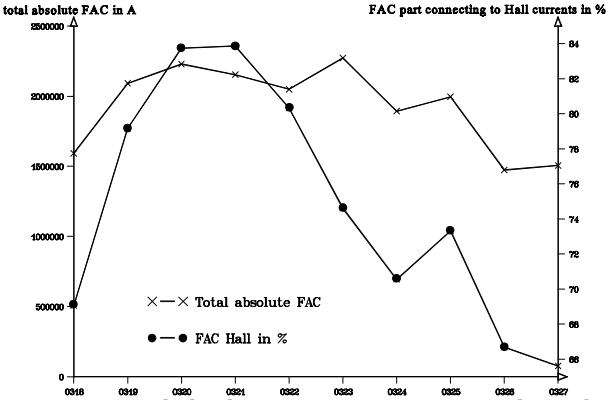


Figure 5. Total absolute FAC in A (crosses, scale on the left side of graph) and percent of FAC connecting to ionospheric Hall currents in % (dots, scale on the right side of the graph) as a function of time over the analysis interval.

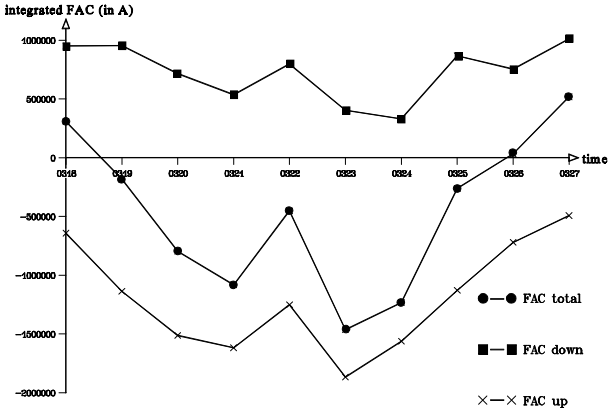


Figure 6. Integrated upward FAC (crosses), integrated downward FAC (squares), and integrated total FAC (dots) in A over the analysis region, as a function of time over the analysis interval.

An interesting open question that arises is how the FAC are balanced and how the current closure in the ionosphere is established. A number of earlier papers assume explicitly or implicitly that the upward and downward FAC associated with omega bands are purely closed by zonally flowing ionospheric currents (e.g., Yamamoto *et al.*, 1993; Lühr and Schlegel, 1994). In this case one would expect that if the FAC are observed in a certain fixed region over which the omega bands are moving in zonal direction, they would balance over one cycle of the omega bands, except for possible small deviations due to effects of partial non-stationarity. Figure 6 shows the integrated upward and downward FAC for each timestep of our analysis (marked by crosses and squares, respectively), and the integrated total FAC (marked by dots). Except for the timesteps 0318 UT, 0326 UT and 0327 UT, the integrated total FAC are upward throughout our event. The upward FAC tend to get larger when the conductance tongue is in the center of the analysis area, with a maximum of ~ 1.9 MA at 0323 UT, while the downward FAC are simultaneously becoming smaller with a mimimum of ~ 0.5 MA at 0324 UT. (An exception is the timestep 0322 UT where part of the FAC structure appears to move out of our analysis region in poleward direction.) Summed up over the whole omega band cycle, an excess of ~ 4.6 MA of upward FAC exists, which is far too large to be explained by any non-stationary effects. This number should be compared with the total of ~ 11.9 MA of upward FAC summed over our analysis period, indicating that the excess of upward FAC amounts to ~ 39%. Therefore we conclude that the FAC cannot be solely closed by zonally flowing ionospheric currents, but part of the upward FAC inside our analysis region have to be connected with downward FAC outside of it by currents flowing in meridional direction. Given the direction of $\vec{E}$, these additional downward FAC regions can only be located poleward of our analysis area.

SUMMARY AND CONCLUSIONS

In this study, we have presented electromagnetic observations from the ground-based MIRACLE and BEAR networks and optical observations from the Polar satellite of an omega band event over Northern

Scandinavia on June 26, 1998, with a special focus on one omega band period from 0318-0327 UT. We have analysed these data using the 2D method of characteristics in combination with a method to derive ionospheric conductances from the UVI and PIXIE data from the Polar satellite, which was here used to estimate the Hall- to Pedersen conductance ratio. The results of this direct and solely data-based analysis allow us for the first time to fully resolve the spatio-temporal evolution of an omega band over one full period with a 1-min time and ~ 50 km spatial resolution.

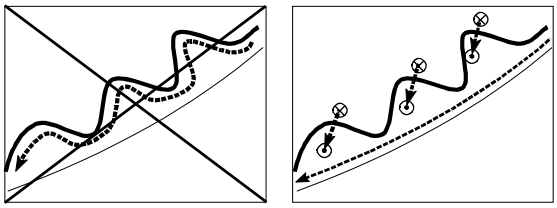


Figure 7. Schematic sketch of the geometry of the westward substorm electrojet within the omega bands: The electrojet is not meandering through the omega band (left panel), but except for a continous part at its base it is intermittently diverted by upward FAC inside the tongues, and fed by downward FAC in the dark areas, thus forming a number of small current wedges (right panel).

Our observations and analysis results can be summarized as follows:

1. The basic properties of the omega bands analysed here agree with the findings of earlier studies. A meandering equivalent current structure moves eastward with a velocity of ~ 770 m s^{-1}, causing magnetic Ps6 pulsations on the ground with a period of ~ 8 min 30 s during the studied interval which are most clearly seen in the Y and Z disturbance components. While no visual band optical observations are available, the UVI images show an eastward moving intensification which is approximately aligned with the westward flank of the region of anticlockwise vorticity of the equivalent currents.

2. Except for the equatorward base region of the omega band, regions of large (up to ~ 60 S) and low (< 5 S) Hall conductance are zonally alternating. The enhanced conductance "tongues" extend ~ 400 km polewards from the base of the omega bands and have a longitudinal extension of ~ 380 km. Steep conductance gradients are present at the zonal and poleward edges of these regions. The conductances in the base region are comparable to the ones in the tongues.

3. The current system of the omega bands can be decomposed into two parts: One part consists of divergence-free Hall currents circulating anticlockwise around the enhanced conductance tongues and of almost radial Pedersen currents which divert to upward FAC of ~ 4 µA m^{-2} in the center of those tongues. This current system causes the characteristic ground magnetic signature and is equivalent to the one proposed by Gustafsson *et al.* (1981). Its sign reverses inside the regions of low conductance. The second part mostly consists of westward flowing curl-free Hall current wedges which divert into strong upward FAC of ~ 15-25 µA m^{-2} at the western flanks of the conductance tongues. Their feeding downward FAC at the eastern flanks of the tongues show magnitudes around ~ 10 µA m^{-2}. These currents are magnetically invisible below the ionosphere. Both current parts mentioned are about equally strong with maximum current densities of ~ 1200 mA m^{-1} and are superposed to the background westward electrojet currents. The geometry of the westward substorm electrojet within the omega bands is schematically sketched in Figure 7.

4. For our event, an overwhelming part (e.g., > 85% at 0323 UT) of the FAC is associated with gradients of the ionospheric conductances, while the remaining part associated with divergences of the electric field is small. Between 66-84% of the FAC is connected with ionospheric Hall currents and controlled by the gradients of the Hall conductance. The total absolute FAC varies between 1.5-2.3 MA and is comparable to the one associated with a WTS. As the upward and downward FAC are not balanced over one omega band period inside our analysis area, we conclude that part of the upward FAC has to be fed by downward FAC located poleward of this area. Thus the closing currents in the ionosphere are not flowing solely in zonal direction, but have an (equatorward) meridional component.

5. While the structures associated with the omega band are moving coherently eastward, they are not strictly stationary.

In addition to the ionospheric point of view, the results of our study have an important impact on the investigation of the ionosphere-magnetosphere coupling of omega bands. In particular our finding that zonally aligned wedges of westward flowing Hall currents exist colocated with the conductance tongues is significant in this respect. These wedges carry a substantial amount of the total westward current and cause zonally alternating FAC which carry integrated currents comparable to a WTS to and from the magnetosphere, and are thus dominating the total FAC pattern of the omega bands. Although this topic is beyond the scope of this paper, we remark that such a situation might be compatible with the suggestion by Jørgensen *et al.* (1999) of large-scale oscillations of the inner edge of the tail current sheet. It would thus be of strong scientific interest to conduct a study like the present one when a multi-satellite magnetospheric mission like Cluster is located in an appropriate conjugate location with the omega bands.

REFERENCES

Akasofu, S.-I., and D.S. Kimball, The dynamics of the aurora; 1. Instabilities of the aurora, *J. Atmospheric Terrest. Phys., 26*, 205, 1964.

Aksnes, A., J. Stadsnes, J. Bjordal, N. Østgaard, R. R. Vondrak, D. L. Detrick, T. J. Rosenberg, G. A. Germany, and D. Chenette, Instantaneous ionospheric global conductance maps during an isolated substorm, *Ann. Geophysicae, 20*, 1181, 2002.

Aksnes, A., J. Stadsnes, G. Lu, N. Østgaard, R. R. Vondrak, D. L. Detrick, T. J. Rosenberg, G. A. Germany, and M. Schulz, Effects of energetic electrons on the electrodynamics in the ionosphere, *Ann. Geophysicae, 22*, 475, 2004.

Amm, O., Direct determination of the local ionospheric Hall conductance distribution from two-dimensional electric and magnetic field data: Application of the method using models of typical ionospheric electrodynamic situations, *J.*

Geophys. Res., 100, 24173, 1995.

Amm, O., Improved electrodynamic modeling of an omega band and analysis of its current system, *J. Geophys. Res., 101*, 2677, 1996.

Amm, O., Method of characteristics in spherical geometry applied to a Harang discontinuity situation, *Ann. Geophys., 16*, 413, 1998.

Amm, O., and Viljanen, A., Ionospheric disturbance magnetic field continuation from the ground to the ionosphere using spherical elementary current systems, *Earth, Planets and Space, 51*, 431, 1999.

Evans, R. D., *The Atomic Nucleus*, McGraw-Hill Book Company , New York, U.S.A., 1955.

Frey, H.U., S.B. Mende, H.B. Vo, M. Brittnacher, and G.K. Parks, Conjugate observations of optical aurora with polar satellite and ground-based cameras, *Adv. Space Res., 23*, 1647, 1999.

Germany, G. A., G. K. Parks, M. Brittnacher, J. Cumnock, D. Lummerzheim, J. F. Spann, L. Chen, P. G. Richards, and F. J. Rich, Remote determination of auroral energy characteristics during substorm activity, *Geophys. Res. Lett., 24*, 995, 1997.

Germany, G. A., G. K. Parks, M. Brittnacher, J. F. Spann, J. Cumnock, D. Lummerzheim, F. J. Rich, and P. G. Richards, Energy characterization of a dynamic auroral event using GGS UVI images, in *Geospace Mass and Energy Flow: Results from the International Solar-Terrestrial Physics Program*, edited by J. L. Horwitz, D. L. Gallagher, and W. K. Peterson, pp. 143, *AGU, 104*, Washington, D. C., 1998a.

Germany, G. A., J. F. Spann, G. K. Parks, M. Brittnacher, R. Elsen, L. Chen, D. Lummerzheim, and M. Rees, Auroral observations from the Polar Ultraviolet Imager (UVI), in *Geospace Mass and Energy Flow: Results from the International Solar-Terrestrial Physics Program*, edited by J. L. Horwitz, D. L. Gallagher, and W. K. Peterson, pp. 149, *AGU, 104*, Washington, D. C., 1998b.

Gjerloev, J, and R. Hoffman, Currents in auroral substorms, *J. Geophys. Res., 107*, doi:10.1029/2001JA000194, 2002.

Gustafsson, G., W. Baumjohann, and I. Iversen, Multi-method observations and modeling of the three-dimensional currents associates with a very strong Ps 6 event, *J. Geophys., 49*, 138, 1981.

Imhof, W. L., K. A. Spear, J. W. Hamilton, B. R. Higgins, M. J. Murphy, J. G. Pronko, R. R. Vondrak, D. L. McKenzie, C. J. Rice, D. J. Gorney, D. A. Roux, R. L. Williams, J. A. Stein, J. Bjordal, J. Stadsnes, K. Njoten, T. J. Rosenberg, L. Lutz, and D. L. Detrick, The Polar Ionospheric X-ray Imaging Experiment (PIXIE), *Space Sci. Rev., 71*, 385, 1995.

Inhester, B., Untiedt, J., Segatz, M., and Kürschner, M., Direct determination of the local ionospheric Hall conductance distribution from two-dimensional electric and magnetic field data, *J. Geophys. Res., 97*, 4073, 1992.

Jørgensen, A.M., H.E. Spence, T.J. Hughes, and D. McDiarmid, A study of omega bands and Ps6 pulsations on the ground, at low altitude and at geostationary orbit, *J. Geophys. Res., 104*, 14705, 1999.

Korja, T., M. Engels, A.A. Zhamaletdinov, A.A. Kovtun, N.A. Palshin, M.Yu. Smirnov, A.D. Tokarev, V.E. Asming, L.L. Vanyan, I.L. Vardaniants, and the BEAR Working Group, Crustal conductivity in Fennoscandia - a compilation of a database on crustal conductance in the Fennoscandian Shield, *Earth Planets Space, 54*, 535, 2002.

Lu, G., A synthetic view of the magnetospheric-ionospheric current system associated with substorms, in *Magnetospheric Current Systems*, AGU monograph, edited by S. Ohtani, R. Fujii, R.L. Lysak, and M. Hesse, 199, 2000.

Lühr, H., and K. Schlegel, Combined measurements of EISCAT and the EISCAT magnetometer cross to study Ω bands, *J. Geophys. Res., 99*, 8951, 1994.

Mravlag, E., M.W.J. Scourfield, A.D.M. Walker, P.R. Stucliffe, and E. Nielsen, Simultaneous observations of omega band related phenomena in both hemispheres, *J. Atmospheric Terrest. Phys., 53*, 309, 1991.

Opgenoorth, H.J., R.J. Pellinen, W. Baumjohann, E. Nielsen, G. Marklund, and L. Eliasson, Three-dimensional current flow and particle precipitation in a westward traveling surge (observed during the Barium-GEOS rocket experiment), *J. Geophys. Res., 88*, 3138, 1983b.

Østgaard, N., J. Stadsnes, J. Bjordal, R. R. Vondrak, S. A. Cummer, D. Chenette, M. Schulz, and J. Pronko, Cause of the localized maximum of X-ray emission in the morning sector: A comparison with electron measurements, *J. Geophys. Res., 105*, 20,869, 2000.

Østgaard, N., J. Stadsnes, J. Bjordal, G. A. Germany, R. R. Vondrak, G. K. Parks, S. A. Cummer, D. L. Chenette, J. G. Pronko, Auroral electron distributions derived from combined UV and X-ray emissions, *J. Geophys. Res., 106*, 26 081, 2001.

Paschmann, G., S. Haaland, and R. Treumann (eds.), *Auroral Plasma Physics*, Kluwer Academic Publishers, Dordrecht, The Netherlands, 2003.

Pulkkinen, A., O. Amm, A. Viljanen, and BEAR working group, Ionospheric equivalent current distributions determined with the method of spherical elementary current systems, *J. Geophys. Res., 108(A2)*, 1053, doi:10.1029/2001JA005085, 2003.

Saito, T., Long period irregular micropulsations, Pi 3, *Space Sci. Rev., 21*, 427, 1978.

Sofko, G.J., R. Greenwald, and W. Bristow, Direct determination of large-scale magnetospheric field-aligned currents with SuperDARN, *Geophys. Res. Lett., 22*, 2041, 1995.

Syrjäsuo, M., T. I. Pulkkinen, R. J. Pellinen, P. Janhunen, K. Kauristie,A. Viljanen, H.J. Opgenoorth, P. Karlsson, S. Wallman, P. Eglitis, O. Amm, E. Nielsen, and C. Thomas, Observations of substorm electrodynamics using the MIRACLE network, *Proc. Fourth International Conference on Substorms (ICS-4)*, Lake Hamana, Japan, March 9 - 13, 1998.

Torr, M. R., D. G. Torr, M. Zukic, R. B. Johnson, J. Ajello, P. Banks, K. Clark, K. Cole, C. Keffer, G. Parks, B. Tsurutani, and J. Spann, A far ultaviolet imager for the international solar-terrestrial physics mission, *Space Sci. Rev., 71*, 329, 1995.

Untiedt, J., and W. Baumjohann, Studies of polar current systems using the IMS Scandinavian magnetometer array, *Space Sci. Rev., 63*, 245, 1993.

Vondrak, R. R., and M. J. Baron, Radar measurements of the latitudinal variation of auroral ionization, *Radio Sci., 11*, 939, 1976.

Vondrak, R., and R. Robinson, Inference of high-latitude ionization and conductivity from AE-C measurements of auroral electron fluxes, *J. Geophys. Res., 90*, 7505, 1985.

Yamamoto, T., K. Makita, M. Ozaki, and C.-I. Meng, A particle simulation of auroral omega bands and torch-like structures, *J. Geomag. Geoelectr., 45*, 619, 1993.